Direct steam reforming of the product gas from ethanol gasification with supercritical water

Athanasios A. Vadarlis [a,*], *Dominik Neukum* [a], *Angeliki A. Lemonidou* [b,c], *Nikolaos Boukis* [a], *Jörg Sauer* [a]

[a] *Karlsruhe Institute of Technology (KIT), Institute of Catalysis Research and Technology (IKFT), Hermann von Helmholtz Platz 1, 76344 Eggenstein Leopoldshafen, Germany*

[b] *Aristotle University of Thessaloniki (AUTH), Department of Chemical Engineering, University Campus, GR 54124 Thessaloniki, Greece*

[c] *Chemical Process Engineering Research Institute (CERTH/CPERI), P.O. Box 6036, Thermi, Thessaloniki, 57001, Greece*

HIGHLIGHTS

- Ethanol supercritical water gasification followed by steam reforming of product gas.
- Increasing temperature, decreasing space velocity increased H_2 yield and CH_4 conversion.
- CH_4 conversion was decreased more at low (1 20 bar) than high (20 40) pressures.
- Excessive steam prevented carbon formation but caused sintering of the active metal.
- Integration of steam reforming reactor increased significantly the total hydrogen yield.

GRAPHICAL ABSTRACT

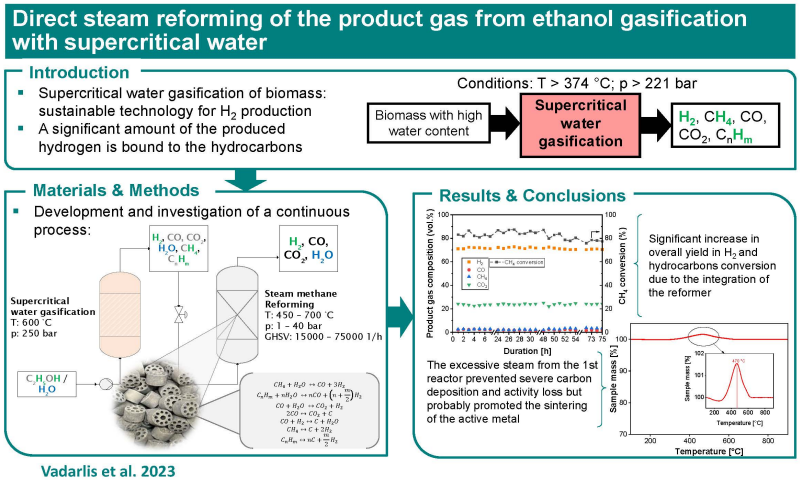

ABSTRACT

A continuous process for producing hydrogen from the gasification of ethanol with supercritical water (SCWG) is investigated, which involves a fixed bed steam methane reforming (SMR) reactor downstream of the SCWG reactor. Increasing temperature and decreasing space velocity in the SMR reactor resulted in increased hydrogen concentration and methane conversion. The catalyst activity was more affected at low than high pressures, presumably due to the kinetics of the SMR reaction. The significant increase in total hydrogen yield based on ethanol in the feed showed the importance of installing the reformer after gasification. The excessive steam from the SCWG reactor helped to prevent

* *Corresponding author*. Karlsruhe Institute of Technology (KIT), Institute of Catalysis Research and Technology (IKFT), Hermann von Helmholtz Platz 1, 76344 Eggenstein Leopoldshafen, Germany.
E mail address: athanasios.vadarlis@kit.edu (A.A. Vadarlis).

Keywords:
Steam methane reforming
Pre reforming
Supercritical water gasification
Ethanol
Ni based catalyst
Hydrocarbons

carbon formation, but it might have resulted in the sintering of the active metal. A long time experiment proved the stability of the catalyst up to 49 h of time on stream (TOS) with a minor decrease in methane conversion from 84% to 78%.

Abbreviations

SCWG	*Supercritical water gasification*
SMR	*Steam methane reforming/reformer*
TOS	*Time on stream*
PR	*Pre reformer/pre reforming*
WGS	*Water gas shift*
GHSV	*Gas hourly space velocity*
BPR	*Back pressure regulator*
TOC	*Total organic carbon*
CGE	*Carbon gasification efficiency*
BET	*Brunauer Emmett Teller*
XRD	*X ray diffraction*
TPR	*Temperature programmed reduction*
TGA MS	*Thermogravimetric analysis coupled with mass spectrometry*
XAS	*X ray absorption spectroscopy*
EXAFS	*X ray absorption fine structure*
XANES	*X ray absorption near edge structure*

1. Introduction

The transition from fossil fuels towards sustainable energy resources relies on the exploitation of technologies that pro duce hydrogen. The increasing amount of hydrogen needed to achieve net zero emissions by 2050 must come from several efficient production pathways [1–3].

The industrial production of hydrogen was based mainly on the steam reforming of natural gas. The chemical reactions that govern this process are the steam reforming of methane (SMR, reaction 1.1) and the water gas shift (WGS) reaction (reaction 1.2) [4]:

$$CH_4 + H_2O \leftrightarrow CO + 3H_2 \quad \Delta H^{298K} \quad 206\frac{kJ}{mol} \tag{1.1}$$

$$CO + H_2O \leftrightarrow CO_2 + H_2 \quad \Delta H^{298K} \quad 41.2\frac{kJ}{mol} \tag{1.2}$$

These two reactions combined give the global reforming reaction, known also as GRM [5]:

$$CH_4 + 2H_2O \leftrightarrow CO_2 + 4H_2 \quad \Delta H^{298K} \quad 164.8\frac{kJ}{mol} \tag{1.3}$$

In this process, side reactions that lead to the formation of coke take place as well. These are the CH_4 decomposition (1.4), the CO reduction (1.5) and the Boudouard (1.6):

$$CH_4 \leftrightarrow C + 2H_2 \quad \Delta H^{298K} \quad 75\frac{kJ}{mol} \tag{1.4}$$

$$CO + H_2 \leftrightarrow C + H_2O \quad \Delta H^{298K} \quad 131\frac{kJ}{mol} \tag{1.5}$$

$$2CO \leftrightarrow CO_2 + C \quad \Delta H^{298K} \quad 172\frac{kJ}{mol} \tag{1.6}$$

The natural gas can contain heavier hydrocarbons that also decompose under the conditions of steam methane reforming [6]:

$$C_nH_m \rightarrow nC + \frac{m}{2}H_2 \tag{1.7}$$

These hydrocarbons can also undergo steam reforming (1.8) and this is done industrially in an adiabatic reactor installed upstream of the main SMR reactor, called pre reformer (PR) [7–9]. There, apart from the steam reforming, the formation of methane via ethane hydrogenolysis takes place (1.9):

$$C_nH_m + nH_2O \rightarrow nCO + \left(n + \frac{m}{2}H_2\right), \Delta H^{298K} \cong 150n + 50\frac{kJ}{mol} \tag{1.8}$$

$$C_2H_6 + H_2 \leftrightarrow 2CH_4, \Delta H^{298K} \quad 187\frac{kJ}{mol} \tag{1.9}$$

An alternative process for hydrogen production based on sustainable resources is the gasification of biomass with supercritical water (SCWG). Under supercritical conditions (T > 374 °C, p > 221 bar) the physicochemical properties of water are drastically altered, i.e., dramatic decrease of its density, viscosity, ion dissociation constant and dielectric constant, making the supercritical water an ideal solvent for non polar organic substances [10]. Under the conditions of supercritical water, the biomass long chain molecules break down to their monomers via hydrolysis. This process can be catalysed by homogeneous or heterogeneous cata lysts [11].

Several chemical reactions take place during the SCWG of biomass. First, the biomass monomers react with the super critical water to form hydrogen and carbon oxides [10]:

$$C_xH_yO_z + (2x \quad z)H_2O \rightarrow xCO_2 + \left(2x \quad z + \frac{y}{2}\right)H_2 \tag{1.10}$$

$$C_xH_yO_z + (x \quad z)H_2O \rightarrow xCO + \left(x \quad z + \frac{y}{2}\right)H_2 \tag{1.11}$$

Then, the product gases react with each other to form mainly methane via methanation of CO (reverse reaction of 1.1) and further hydrogen and carbon dioxide via the WGS reaction (reaction 1.2). Reactions that lead to coke take place as well. These are the 1.4–1.7 but also the decomposition of intermediates (1.12),

$$C_xH_yO_z \rightarrow Coke \tag{1.12}$$

The SCWG of biomass generates a product gas that consists of H_2, CH_4, CO_2, CO and other hydrocarbons (mainly C_2–C_3) [12,13]. In many cases, a significant amount of the produced hydrogen from SCWG is bound in the hydrocarbons formed. To maximize pure hydrogen gas, a downstream upgrading process is necessary (SMR), which will transform the bound hydrogen into molecular H_2 [14]. Several authors have stated the importance of implementing a secondary reactor for the steam reforming of the hydrocarbons into further hydrogen production [13–15].

Most of the studies dealing with the upgrading of the product produced by gasification of biomass focussed on experimentally exploring the subsequent steam reforming of tar produced by biomass gasification [16–21]. However, the gasification in all studies was under atmospheric pressure. Gramms et al. [22] investigated the steam reforming of biomass pyrolysis vapors with a Ni based zeolite catalyst. Sun et al. [23] used a Ni based volcanic rock catalyst for steam and dry reforming of a gas mixture produced from gasification of pine nutshell.

There has been considerable work in literature regarding the simulation of processes that combine the SCWG of biomass resources with steam methane reforming. Rahbari et al. [24] carried out a simulation and techno economic analysis of the integration of a steam reformer into a micro algae SCWG process with heat provided by solar energy. Ruya et al. [25] simulated and studied the exergy loss for the SCWG of empty fruit branch and palm oil mill with an integrated steam methane reformer. Zhang et al. [26] considered a sorption enhanced gasification of biomass utilizing the captured CO_2 for dry methane reforming. Recently, Hantoko et al. [27] designed a process that combined glycerol SCWG and a SMR reactor, which operated at the same pressure with the SCWG reactor (250 bar). From their simulation, they found that the implementation of a steam reformer resulted in increased H_2 yield and syngas production.

The scope of this work is to explore the potential of the combined process of biomass SCWG and steam reforming of the product gas experimentally with a target to maximize hydrogen yield. Since this work is a proof of concept, no real biomass was used but a substance that models biomass waste with high water content, i.e., ethanol dissolved in water. This process combines the SCWG of aqueous ethanol solutions with a subsequent downstream steam reforming fixed bed reactor for the conversion of methane and any traces of heavier hydrocarbons produced in the SCWG reactor, like a pre reformer. The feed is directly fed to the second reactor, which utilizes all the water left from SCWG to steam reform the dry product gas. This excess steam may differentiate the operation from that of conventional steam methane reforming (SMR) processes. For instance, carbon formation is expected to be minimized, as the excess amount of steam leads to high steam to carbon (S/C) ratios compared to the typical range. This, in turn, allows for lower temperatures to achieve complete methane reforming. Thus, the current study incorporated also lower reforming temperatures, as low as 450 °C, which is close to the lowest value of 400 °C found in the literature [8,28–31]. This work aims to investigate how the primary operating parameters, including temperature, pressure, and residence time in the SMR reactor, affect the performance of this reactor, in terms of product composition and specifically methane conversion and hydrogen yield. Furthermore, the heterogeneous catalyst used in the process is characterized to identify any morphological and structural changes that may occur during the reaction.

2. Materials and methods

2.1. *Experimental setup*

The feeding system consists of a vessel containing an ethanol/water solution, a scale and an HPLC pump (Bischoff Model 2250). A capillary tubing connects the pump outlet with the entrance of the SCWG reactor. The reactor (I: SCWG) is made from nickel based alloy 625. It is 1000 mm long, with an inner diameter of 8 mm. Heat is provided to reactor I through three heating coils in spiral form, located in series at the outer wall of the reactor. The temperature across the reactor is monitored and regulated by six thermocouples. The pressure in this reactor is regulated by a back pressure regulator capable of operating at temperatures as high as 500 °C (Equilibar, ULHT Series Precision, Pressure Control Solutions) and is set at 250 bar. Temperature losses in the small lab scale layout are very high, thus several heating devices are necessary to avoid cooling of tubes and back pressure regulator below 380 °C. A heating coil is installed to the bottom of the back pressure regulator. Another heating coil is used to heat the pipe between the SCWG reactor and the pressure regulator and keep its temperature around 500 °C so that the condensation of water does not occur.

The second reactor (II) is installed on top of the back pressure regulator and is connected to the outlet port of it so that the product gas from the first reactor is directly led into the second reactor. This reactor is also made from nickel based alloy, its length is 800 mm, and its inner diameter is 8 mm. For its heating, three heating coils are used. A thermocouple is placed vertically in the center of the reactor to measure the temperature of the catalytic bed.

The catalytic bed consists of the catalyst particles (250–500 μm), and it is supported by a metallic net and quartz wool. The catalyst used is the ReforMax 210 LDP, a commercially available one (purchased from C&CS catalysts and chemicals specialties GmbH) based on NiO (18 wt%) and supported on a $CaK_2Al_{22}O_{34}$ support. The quantity of the catalyst is adjusted according to the desired Gas Hourly Space Velocity (GHSV in h^{-1}) of each experiment. The GHSV is calculated from the following equation:

$$GHSV \quad \frac{(Q_{reactants})^{ambient\ conditions}\left(\frac{m^3}{h}\right)}{V_{cat.\ bed}\ (m^3)} \tag{2.1}$$

The volumetric flow of the reactants, $Q_{reactants}$, is the volumetric flow of the SCWG product under ambient conditions. The volume of the catalytic bed, $V_{cat.\ bed}$, is defined as the quotient of the mass of the catalyst, m_{cat}, to its apparent density $d_{cat.}$:

$$V_{cat.\ bed} \quad \frac{m_{cat.}}{d_{cat.}} \tag{2.2}$$

The apparent density of the catalyst was measured to be equal to 0.915 g/mL.

The product stream exiting the second reactor, is driven to a gas sampling bulb, a liquid gas separator, and a gas meter (type TG0.5/7, provided by Ritter). The liquid condensate is separated from the product gas and is collected in the phase separator, where its weight is also measured by a scale. Fig. 1 depicts the system described above. An intermediate gas sampling point consisting of three valves (V02, V03, V04) and a gas bulb are installed for measuring the product gas composition from the first reactor.

2.2. Experimental procedure

Initially, a mixture of H_2 (20 vol%)/N_2 gas, which acts as a reducing agent for the active metal phase, is introduced to the catalyst bed for 2 h with a flow of 50–60 mL/min, at 700 °C and ambient pressure. While the reduction of the catalyst is conducted, the first reactor is heated up at 600 °C (desired value for SCWG). Next, water is added to the system with a flow of 1 mL/min, until the pressure in the first part of the system reaches its desired value of 250 bar. After this step, feed is introduced to the system with a volumetric flow rate of 1.6 mL/min. The ethanol concentration in the feed was 8 wt%. The operating temperature of the reactor I was set at 600 °C in all experiments. Different temperatures in the catalytic bed reactor II were studied, from 450 °C to 700 °C with an increment of 50 °C. Different pressures in the second reactor were also studied, in the range 1–40 bar. This range corresponds to that applied in industry for hydrogen and syngas production [32–34]. The GHSV received the following values: 14852 h^{-1}, 22234 h^{-1}, 29665 h^{-1}, 44557 h^{-1}, 59331 h^{-1} and 74163 h^{-1}.

During each experiment, every half hour, a gas sample was taken for analysis in a Gas Chromatograph (Hewlett Packard Series II 5890 Plus model) equipped with a thermal conductivity and flame ionization detectors and a silica capillary column (Carboxen 1010 PLOT 30 m, SUPELCO). Samples from the feed and from the liquid effluent are analyzed in a DIMATOC 2100 (DIMATEC), so that the total organic carbon (TOC) content of both can be determined.

Prior to the experiments combining the two reactors, several experiments with only the SCWG system were conducted, to define the input to the pre reforming reactor. The conditions of those experiments were: p 250 bar and T 600 °C. Ethanol with an 8 wt% concentration was used with a volumetric flow of 1.6 mL/min. It should be noted here that the first reactor was previously used for the same application but with 50 ppm K^+ by adding $KHCO_3$. This was done in order to study its effect on ethanol gasification. However, in this experimental study, no K^+ addition was performed. In section 3.1, the effect of K^+ is explained in more detail, and why it is necessary to refer to it. Although the reactor has a total length of 1000 mm, the heated part accounts for 650 mm; thus, only this length was considered for the residence time calculation. The value of the latter parameter at experimental conditions (600 °C, 250 bar) was thus steady at 1.51 min. The TOC content of the liquid effluent is determined here as well.

The parameters used for the evaluation of the performance of the SCWG process are the Carbon Gasification Efficiency (CGE):

$$CGE(\%) \quad \frac{n_{C\ in\ product\ gas}}{n_{C,feed}} \tag{2.2.3}$$

and the yield of product gases:

$$Y_i\left(\frac{mol}{mol_{ethanol}}\right) \quad \frac{n_i(mol)}{n_{ethanol\ in\ feed}(mol)}, i \quad H_2, CH_4, CO_2, CO\ and\ C_{2+} \tag{2.2.4}$$

The steam to carbon ratio (S/C) of the SCWG product was calculated with the following equation:

$$\frac{S}{C} \quad \frac{\dot{n}_{H_2O,outlet}\left(\frac{mol}{h}\right)}{\dot{n}_{CH_4,outlet} + \dot{n}_{CO_4,outlet} + \dot{n}_{CO,outlet} + 2\cdot\dot{n}_{C_2H_6,outlet} + 3\cdot\dot{n}_{C_3H_8,outlet}\left(\frac{mol}{h}\right)} \tag{2.2.8}$$

The hydrocarbons higher than methane that are expect to be produced are C_2H_6 and C_3H_8. The parameters that are used for studying the performance of the pre reforming catalyst are the conversion of methane and the yield of hydrogen. The CH_4 conversion is defined as:

$$CH_4\ conversion\ (\%) \quad \frac{CH_{4,inlet} \quad CH_{4,outlet}(mol)}{CH_{4,inlet}(mol)} \tag{2.2.5}$$

The yield of H_2 according to the Global reforming reaction of methane (GRM) (1.3) is also used for the evaluation of the performance of the steam reforming reaction:

$$H_2\ yield\ (\%) \quad \frac{H_{2,outlet} \quad H_{2,inlet}(mol)}{4\cdot CH_{4,inlet}(mol)} \tag{2.2.6}$$

where, $H_{2,outlet}$ and $H_{2,inlet}$ denote the moles of hydrogen in the product and in the reactant of the second reactor, respectively.

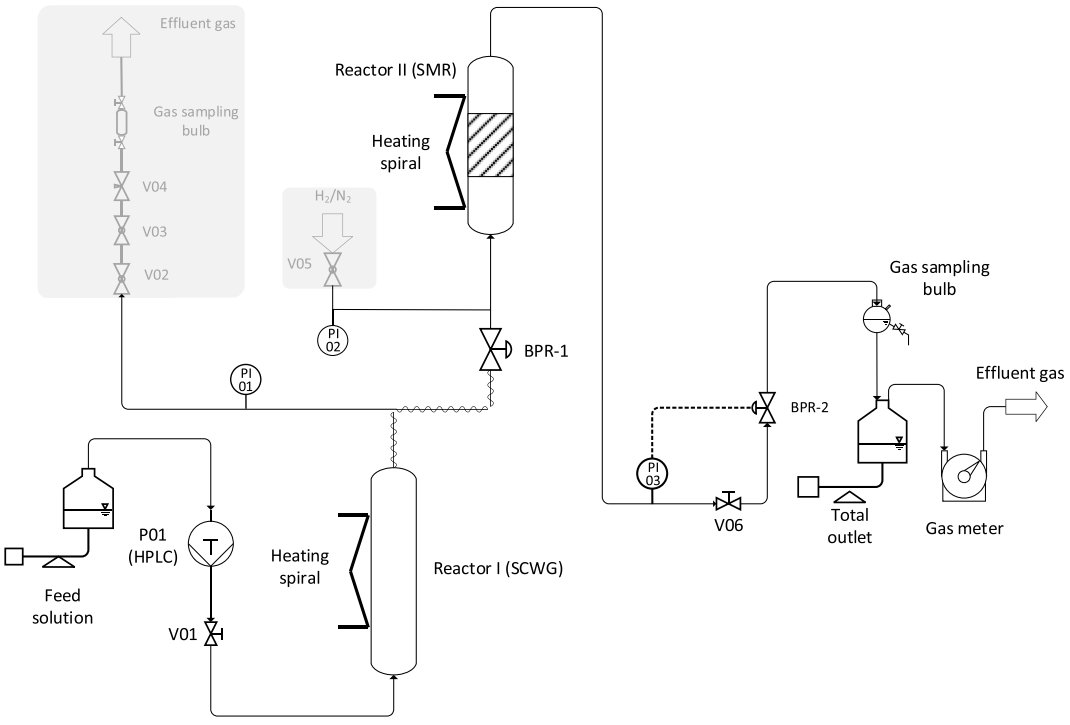

Fig. 1 – Experimental layout. "BPR" is an abbreviation of "Back-pressure regulator". The gray areas identify the parts of the layout which are not part of the main function of the installation but belong to ancillary equipment.

Three equations are used to compare the yield of H_2 from SCWG to the additional respective yield from steam reforming. The first (2.2.8) is the yield from SCWG, the second (2.2.9) from steam reforming, and the total yield (2.2.10) is the third one, which accounts for the total hydrogen produced based on ethanol, according to reaction 2.2.7 [35]:

$$C_2H_5OH + 3H_2O \leftrightarrow 6H_2 + 2CO_2, \Delta H^{298K} \quad 173.5\frac{kJ}{mol} \tag{2.2.7}$$

$$Y_{H_2,SCWG}(\%) \quad \frac{\dot{n}_{H_2,SCWG}\left(\frac{mol}{h}\right)}{6\cdot\dot{n}_{Ethanol}\left(\frac{mol}{h}\right)} \tag{2.2.8}$$

$$Y_{H_2,SR}(\%) \quad \frac{\Delta\dot{n}_{H_2}\left(\frac{mol}{h}\right)}{6\cdot\dot{n}_{Ethanol}\left(\frac{mol}{h}\right)}, \Delta\dot{n}_{H_2} \quad \dot{n}_{H_2,total} \quad \dot{n}_{H_2,SCWG} \tag{2.2.9}$$

$$Y_{total}(\%) \quad \frac{\dot{n}_{H_2,total}\left(\frac{mol}{h}\right)}{6\cdot\dot{n}_{Ethanol}\left(\frac{mol}{h}\right)} \tag{2.2.10}$$

where $\dot{n}_{Ethanol}$ is the amount of ethanol in the feed to the system, $\dot{n}_{H_2,SCWG}$ is the amount of H_2 produced from SCWG and $\dot{n}_{H_2,total}$ the total amount of H_2 produced from the whole process, which can be calculated by the flow of gas coming from the reformer.

Before studying the effect of a parameter in the reformer, at least one experiment was carried out, which involved the SCWG of 8 wt% ethanol. This was done to observe any changes in the SCWG system that affect the CGE, the yield and the composition of the product gases. The mass and carbon balances were also taken into consideration for every experiment, not only for the SCWG experiments, but also for the experiments of SCWG and subsequent steam reforming. The mass balances ranged from 93% to 101%, while the range of the carbon balances was 95–107%.

2.3. *Characterization of fresh and used catalysts*

The Brunauer Emmett Teller (BET) surface area and porosity of both fresh and reduced samples of the catalyst were determined by N_2 physisorption at 77 K with an Autosorb 1 (Quantachrome, Florida, UK) flow apparatus, installed in the Chemical Process & Energy Resources Institute (CPERI) of Center of Research and Technology Hellas.

A gas flow system equipped with a quadrupole mass analyzer (OMNIStarTM, PFEIFFER, Germany) was used for the H_2 temperature programmed reduction (TPR). 0.15 g of catalyst were placed in a U shaped quartz reactor and treated with He gas at 250 °C for 0.5 h, followed by cooling to room temperature. The temperature was raised afterwards from room temperature to 800 °C at a rate of 10 °C/min in a gas mixture containing 10% H_2/He. During the experiment, the following mass to charge ratios were recorded: He 4, H_2 2, and H_2O 18. All measurements were carried out with an automated flow unit located in the Laboratory of Petrochemical Technology, at the Chemical Engineering Department, AUTh. The unit is equipped with Genie Advantech software that controls all functions and has two identical groups of gas inlet lines, each with four lines and an equal number of electronic flow controllers (Brooks Smart).

Powder diffractograms of the catalyst were obtained with a PANalytical X'Pert Pro diffractometer using Cu K_α radiation and a Ni filter. The data was recorded in a step size of 0.033° with 2θ ranging from 5 to 120°. The full width at half maximum of the 111 reflection of nickel (44.5°) was deter mined by peak fitting with Origin2019. The FWHM was used to estimate the domain size using the Scherrer equation and LaB_6 as reference.

For thermogravimetric analysis coupled with mass spec trometry (TGA MS), about 40 mg of the sample were filled into a small crucible. The sample was flushed with 80 mL of Ar containing 10% O_2 for approximately 8 h. Afterwards the sample was heated with 5 °C/min to 1100 °C in the same flow. The gas concentration was monitored with a Netzsch QMS 403 D Aeolos. Background correction with an empty crucible was performed. The data were analyzed with Origin2019. For the measurements a Netzsch STA 449 F^3 Jupiter was used.

X ray absorption spectroscopy (XAS) of the fresh and spent catalyst, as well as Ni foil reference were conducted at the P65 beamline at PETRA III (Deutsches Elektronen Synchrotron, Hamburg) at Ni K edge (24.35 keV). They were performed in transmission mode using ionization chambers. The radiation came from an 11 period undulator. The energy was selected using a Si(111) double crystal monochromator. A pair of plane Si mirrors rejected higher harmonics. The beam size was 1.5 × 0.3 mm for all samples. Powder samples were measured as pellets diluted with cellulose. The data analysis was carried out using Athena from the Demeter software package (version 0.9.26).

3. Results and discussion

3.1. Determining the product from the SCWG reactor

As mentioned in section 2.2, the composition of product from the SCWG reactor was first determined. The average values of the dry product gas composition and the yields of product gases from the SCWG of an 8 wt% ethanol water solution are given in Table 1. This table shows that the most abundant gas is H_2, and the second is CH_4. The content of carbon monoxide was found equal to around 6 vol%. The hydrocarbons higher than methane account for approximately 1 vol% of the dry product gas. These hydrocarbons consist mainly of ethane. On average, 16.6 L/h of dry gas is produced. The aqueous effluent is in the range of 4.5–5.0 mol/h. The carbon found in the aqueous effluent is 90–160 ppm. Practically, all the carbon content in the feed is gasified, i.e., the CGE was in the range of 99.6–99.9%. From Eqn 2.2.8 the $Y_{H2,SCWG}$ is equal to 27.4%. The S/C ratio of the feed to the second reactor is 11.28–13.50. This composition, together with the average S/C ratio (12.39) and the average molar flows of the gases and steam are considered as feed to the second reactor.

These data must be interpreted cautiously because, in the initial phase of the experiments, the gasification was conducted by adding 50 ppm K^+, by adding $KHCO_3$. K^+ acts as a homoge neous catalyst in SCWG of organic substances by promoting the WGS reaction [36]. Thus, with the addition of K^+, in the product gas from the SCWG of 8 wt% ethanol, the CO concentration was around 1.4 vol%. During these initial experiments the concen tration of the C_{2+} hydorcarbons was around 5 vol%. After around 70 h of operation with K^+, the concentration of C_{2+} hy drocarbons decreased to 0.5–1 vol% and was steady afterwards. After performing experiments without adding $KHCO_3$, the concentration of C_{2+} hydrocarbons was constant at the afore mentioned levels. These findings suggest that the surface of the SCWG reactor's inner walls was altered permanently. In a study that aimed to determine the effect of potassium salts in SC water on a Ni based alloy 625, Habicht et al. [37] found that these salts can corrode the surface of this metal and result in the formation of areas on reactor's surface rich in NiO. During SCWG of ethanol, H_2 can reduce NiO and form metallic Ni, active in steam reforming of C_{2+} hydrocarbons.

3.2. Characterization of fresh catalyst

The BET surface area of the fresh and reduced catalyst is given in Table 2. The reduced one had higher surface area, pore volume, and diameter than the fresh one. However, the sur face area of the reduced catalyst is still considered low due to the low surface area of the support used [38].

The reduction pattern of the fresh catalyst was studied over a temperature range of 50–800 °C. The volumetric flow of hydrogen over the catalyst sample as a function of tempera ture is given in Fig. 2. The drop in the flow of H_2 is due to its consumption in the reducing reaction of NiO to form Ni^0, as the XRD patterns of the fresh and reduced catalyst depicted (in Fig. 3). In the temperature range 400–590 °C, the H_2 flow begins to decrease and is minimized around 508 °C. A small con sumption is still around 615 °C before the flow returns to pre consumption levels. These temperatures agree with those from the literature [29,38–41], leading to the conclusion that this catalyst is easily reduced. This fact can be attributed to the weak interaction between the active metal and the sup port [38,41]. By calculating the theoretical and the experi mental consumption of H_2, it is estimated that approximately 98.7% of Ni^{2+} is reduced.

Table 1 – Dry gas composition and yields of the product gases from the SCWG of 8 wt% ethanol at 600 °C and 250 bar.

	Concentration (vol%)	Yield ($mol/mol_{ethanol}$)
H_2	43	1.64
CH_4	28	1.06
CO	6	0.23
CO_2	22	0.82
C_{2+}	1	0.04

Table 2 – Physicochemical properties of fresh and reduced catalyst.

	BET surface area (m^2/g)	Pore Volume (cm^3/g)	Pore diameter (nm)
Fresh catalyst	3.8	0.025	9
Reduced catalyst	14.6	0.039	12

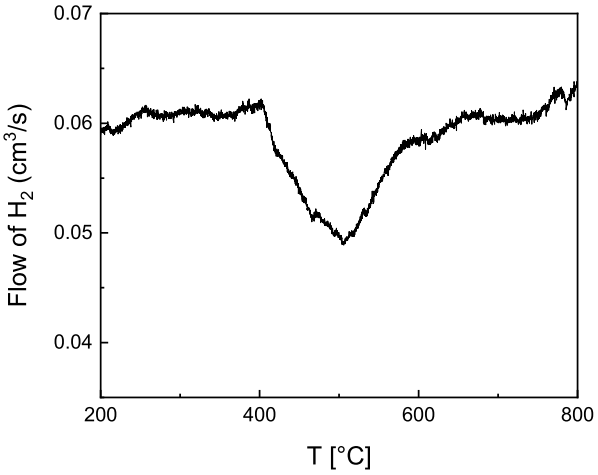

Fig. 2 – H_2 -TPR profile of the fresh catalyst.

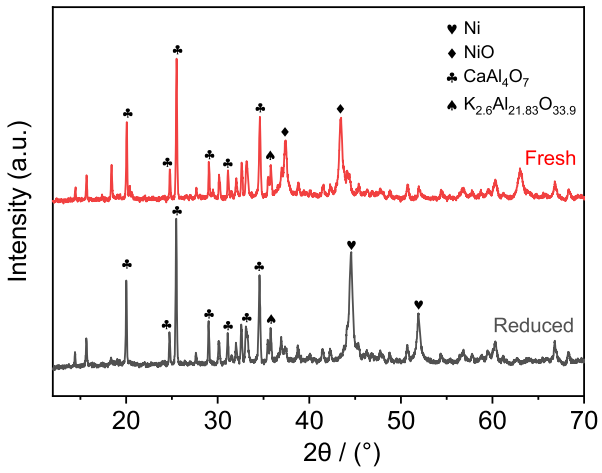

Fig. 3 – XRD graphs of the fresh and reduced catalyst.

The X Ray diffractograms of the fresh and reduced catalyst are presented in Fig. 3. Both samples consisted of $CaAl_4O_7$ and $K_{2.6}Al_{21.82}O_{33.9}$ crystal phases, the former in significantly higher intensity implying that it is the main support component. The similarity in the intensity of the reflections of the support crystal phase between the fresh and the reduced samples ensures that they have not undergone any structural changes due to the reduction of the active metal. Regarding the Ni phases, the fresh sample shows diffraction peaks of NiO, while the reduced one shows only those corresponding to metallic Ni. This indicates that the reduction conditions were sufficient for converting Ni^{2+} to Ni^0. The size of the Ni crystallites in the reduced catalyst was calculated by the Scherrer equation and was found to equal 35.8 nm. This value is later compared with the respective size of the Ni crystallites after the reaction to examine whether Ni sintering had taken place.

3.3. *Thermodynamic equilibrium*

The catalytic performance of the pre reforming catalyst is compared with the dry gas composition at thermodynamic equilibrium. The latter composition is calculated from the Aspen HYSYS V11, with an RGibbs reactor chosen to minimize the Gibb's free energy of the system [42]. The selected property package was the PRSV, which employs the Peng Robinson equation. The product gas composition and CH_4 conversion were determined under varying temperatures of 450–700 °C and atmospheric pressure (Fig. 4a), as well as under a pressure range of 1–41 bar and a constant temperature of 600 °C (Fig. 4b). The product composition from the SCWG of an 8 wt% ethanol solution, as shown in Table 1, was used as feed for the thermodynamic equilibrium calculations.

The effect of temperature on dry gas equilibrium composition is illustrated in Fig. 4a. The concentration of hydrogen increased while that of methane decreased due to the promotion of the SMR reaction [8,27]. Conversely, WGS was promoted at lower temperatures, as shown by the lower carbon monoxide concentration because of its consumption towards CO_2 and H_2. At 700 °C, almost complete CH_4 conversion was calculated, and H_2 reached its highest concentration of 73.5 vol%. The determined conversion of C_{2+} hydrocarbons was complete across all temperature and pressure ranges.

Pressure as expected has a strong inverse effect on CH_4 conversion due to the promotion of the methanation reaction, which inhibits the formation of CO and H_2 (Fig. 4). At 20 bar the

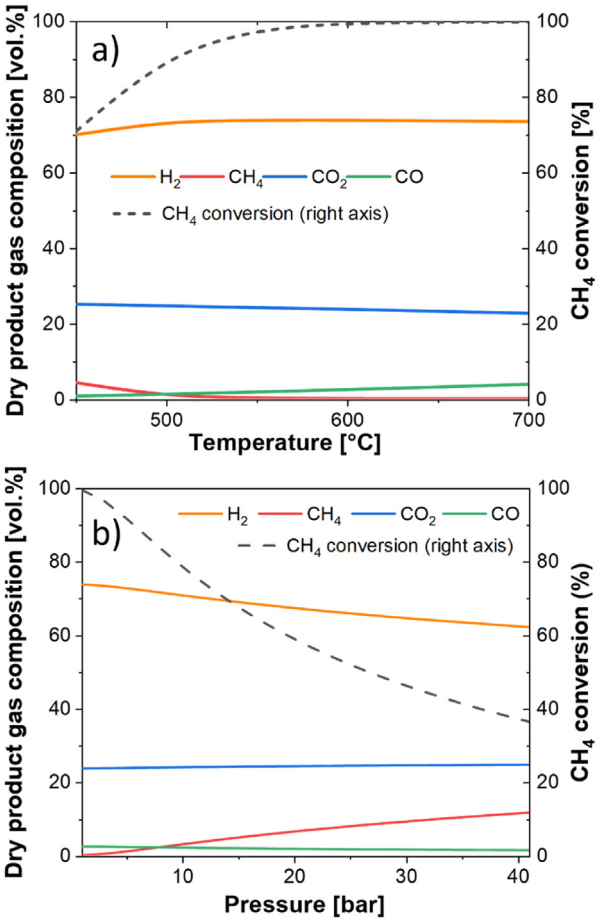

Fig. 4 – a) Effect of temperature and b) of pressure on the equilibrium composition of the dry product gas (vol%) from steam reforming of the gas generated from the SCWG of 8 wt% ethanol. The SCWG product gas corresponds to the values of Table 1.

conversion is less than 60%. As WGS reaction is a reaction with no volume change, it is not affected by pressure. The variation seen mostly in H_2 concentration is due to the steadily increasing CH_4 concentration.

3.4. *Effect of temperature on the steam reforming product*

The experimental study first includes the effect of tempera ture on the dry product gas composition and the catalyst's performance in terms of CH_4 conversion and H_2 yield. Fig. 5 depicts the concentration of the product gases as a function of catalyst bed temperature and the corresponding composi tion at thermodynamic equilibrium. It can be seen that H_2 concentration is increasing with temperature, from 57 vol% at 450 °C to almost 70 vol% at 700 °C. Respectively, the concen tration of CH_4 decreased from 22 vol% to 7 vol%. The CO concentration was minimized at 450 °C, where it was 0.05 vol % but increased up to 3.2 vol% approximately, at 700 °C. This trend shows the strong effect of temperature on the reactions of SMR and WGS. The WGS reaction is promoted at low tem peratures since it is exothermic, whereas higher temperatures forward its reverse reaction [43]. Therefore, with a tempera ture increase, the content of CO is increased. On the other hand, the endothermic SMR reaction is shifted towards the generation of H_2 and CO when the temperature rises, whereas it is shifted towards CH_4 and H_2O when the temperature de creases. At 450 °C, the C_{2+} hydrocarbons made up 0.6% of the dry product gas, while at 700 °C they accounted for only 0.03%. Although they were present in small amounts, there was a noticeable pattern of increasing conversion as the tempera ture increased, as demonstrated in Fig. 5.

As shown in Fig. 5a), a significant deviation from the thermodynamic equilibrium exists, especially at lower tem peratures. For high temperatures, the actual product gas composition reaches closer to the equilibrium. A significant deviation from the equilibrium is found for CH_4 concentration. Even at 450 °C, the CH_4 decreases drastically under thermo dynamic equilibrium, reaching approximately 4.3 vol%, due to the very high S/C ratio that drives the reactions of SMR and WGS to the side of H_2 formation. However, no significant in crease in CH_4 conversion was found experimentally at 450 °C. The reaction rate of the SMR reaction is influenced strongly by the temperature, due to the high activation energy of this re action. Xu et al. [44] for example, found an activation energy of 240.1 kJ/mol for a Ni/$MgAl_2O_4$ catalyst, while Obradovic et al. [45] found a slightly higher value (247.3 kJ/mol) for a structured plate type Pt/Ni/Al_2O_3 catalyst. Abbas et al. [46] calculated the activation energy of a NiO(18 wt%)/Al_2O_3 to be equal to 257 kJ/ mol.

Consequently, the conversion of CH_4 and the yields of H_2 and CO were also expected to have a strong temperature dependence. Fig. 5b) reveals that there has been a gradual increase in the conversion of CH_4 from around 13.8% at 450 °C to 63.3% at 700 °C. A similar trend was found for the H_2 yield (2.2.6), where it was around 18.2% at the lowest tem perature, reaching approx. 59% at the highest temperature, respectively. The conversion of higher hydrocarbons in creases with temperature as well, from around 32% at 450 °C to 95% at 700 °C. Both graphs show that at low and moderate

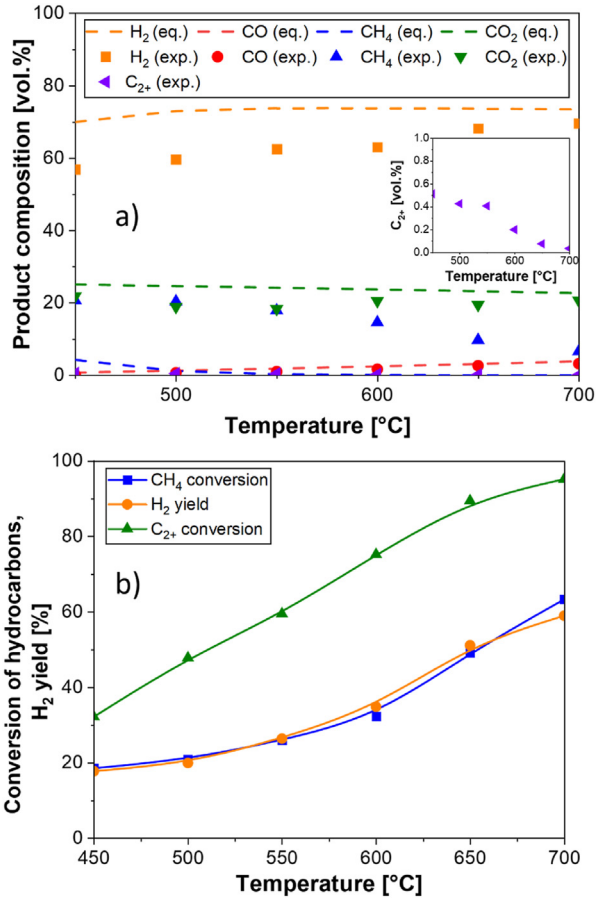

Fig. 5 – a) Dry product gas composition with temperature in the steam reforming reactor, compared with thermodynamic equilibrium, b) Conversion of hydrocarbons and hydrogen yield with temperature. The pressure was atmospheric, the feed was the gas from SCWG of 8 wt% ethanol (see Table 1), and GHSV was around 74163 h^{-1}.

temperatures the activity of the catalyst increases slightly with temperature, whereas at temperatures higher than 600 °C, the total increase in activity is remarkably steeper. Similar results were found by Yang et al. [47], who reported a 3 fold increase in CH_4 conversion from 550 °C to 650 °C, for SMR with an S/C ratio of 3 and CH_4 space velocity of 10^4 h^{-1} over a Ni–Ce/Al catalyst. Other researchers found a gradual noteworthy increase in H_2 yield from 500 °C to 700 °C, higher than the one of this study, probably due to the lower GHSV applied [48] and/or the higher activity of the catalyst used [29].

The yield of hydrogen from the SCWG ($Y_{H2,SCWG}$) is calcu lated from Eqn 2.2.8 to equal 27.4% and is considered steady during the variation of temperature in the second reactor, since no changes occurred in the first reactor. At the lowest applied reforming temperature, i.e. 450 °C, the $Y_{H2,SR}$ 18.9%, while the Y_{total} was 46.3%. At the highest temperature, i.e. 700 °C, the total hydrogen yield increased to 76.6% due to the in crease in the $Y_{H2,SR}$ to 49.2%. At low temperatures, the $Y_{H2,SR}$ is lower than the $Y_{H2,SCWG}$ but increases significantly with

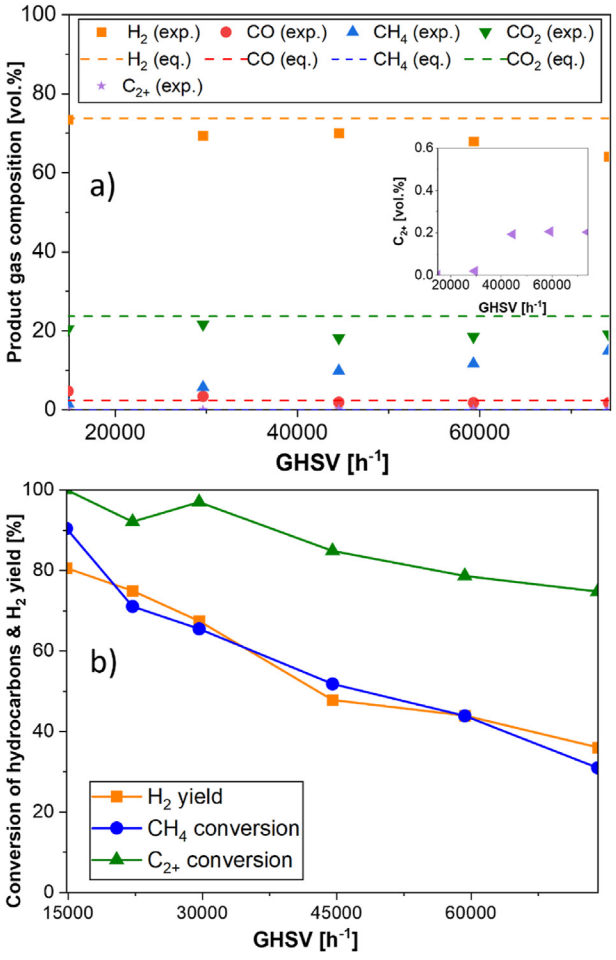

Fig. 6 – a) Product gas composition with GHSV in the steam reforming reactor, b) Conversion of CH_4 and H_2 yield with GHSV The feed was the product from the SCWG of 8 wt% EtOH (see Table 1), pressure was atmospheric and T 600 °C.

temperature. At temperatures of 600 °C and higher, the $Y_{H2,SR} > Y_{H2,SCWG}$.

3.5. *Effect of GHSV*

In a previous section, it was observed that a substantial de viation from thermodynamic equilibrium occurred at a GHSV of 74163 h^{-1}, even at high temperatures (T > 600 °C). The actual methane conversion was found to be only 32%, whereas the theoretical value was almost 100%. Conse quently, the effect of GHSV needed to be investigated further, and a temperature of 600 °C was selected for this purpose. The feed was the product gas from the SCWG of 8 wt% ethanol. The values from Table 1 were used to describe the feed to the second reactor, regarding the SCWG product gas composition, the S/C ratio and the molar flows of all components.

The impact of GHSV on the product gas composition is shown in Fig. 6. The concentration of H_2 reaches almost its equilibrium value at the lowest GHSV, i.e., 73.4 vol%. Higher GHSVs as expected, cause a deviation from the equilibrium. Additionally, the concentration of CH_4 increases with GHSV, reaching its lowest value of 1.48 vol% at a GHSV of 14852 h^{-1}. The concentration of CO_2 remains constant and slightly lower than the equilibrium value. However, the concentration of CO was 3.36 vol% and 4.68 vol% at GHSVs of 22234 h^{-1} and 14852 h^{-1}, respectively, while the equilibrium CO concentration is around 2.43 vol%. It is possible that with increase in GHSV, the reverse WGS reaction is promoted [41,49]. The level of C_{2+} hydrocarbons remained steady at approximately 0.2 vol% when the GHSV was between 44557 and 74163 h^{-1}, but then their concentration dropped below 0.02 vol%, and at the lowest GHSV, they were not detectable. No signs of catalyst deactivation were observed throughout the studied range of GHSVs. Similarly, the CH_4 conversion shows a dramatic in crease at lower GHSVs. Its highest value was approx. 90.4%, at GHSV of 14852 h^{-1}. The respective value of the H_2 yield (2.2.6) was 80.5%.

The GHSV is an essential parameter for the performance of this process [30]. At the studied temperature of 600 °C, the CH_4 conversion and H_2 yield (Eqn 2.2.6) were considerably dependent to the GHSV, consistent with the observations of previous researchers [50]. The GHSV is inversely related to the residence time. Higher GHSVs result in lower residence times, i.e., shorter contact times between the reactants and the catalyst, negatively affecting the conversion of CH_4 and the H_2 yield [46]. Apart from that, high GHSVs can result in more rapid activity losses, as Zhai et al. [51] demonstrated. Additionally, there are critical residence time values, above which thermodynamics controls the outcome of the pro cess, whereas lower values lead to control by reaction ki netics [52].

Here, at the lowest GHSV, the hydrogen yield based on reforming of the intermediate stream (Eqn 2.2.9) is $Y_{H2,SR}$ 70.6% while total H_2 yield based on the ethanol fed to the reactor (Eqn 2.2.10) approaches 98%. Through the entire range of applied space velocities, the $Y_{H2,SR}$ was higher than $Y_{H2,SCWG}$, which was considered stable at 27.4%.

3.6. *Effect of pressure*

The effect of the pressure (1–40 bar) on the dry product gas composition (Fig. 7a), CH_4 conversion and H_2 yield (Eqn 2.2.6) (Fig. 7 b) in the downstream steam reforming reactor was also investigated. It strongly affects CH_4 concentration which rises gradually, from 4.13 vol% at 1 atm, to 12.3 vol% at 40 bars and H_2 which is reduced from 70.5 vol% at atmospheric pressure, to 61 vol% at 40 bar. Similarly, CO decreases from 4.26 vol% to 1.7 vol%. A slight increase in CO_2 concentration, from 21 vol% at 1 atm, to 24.9 vol% at 40 bar is also observed. The increase in pressure forwards the reverse SMR reaction, resulting in higher CH_4 concentration and lower CO and H_2 concentrations [50]. Although the CO_2 concentration rose slightly with pres sure, the overall effect of pressure on the WGS reaction was small compared to the SMR reaction. The WGS has equal amount of moles on its both sides, and when it reaches equilibrium is not affected by pressure [46,50,53]. In this case, the SMR is inhibited with pressure and so this excess amount of steam reacts further with the CO, driving the slight rise in CO_2 concentration.

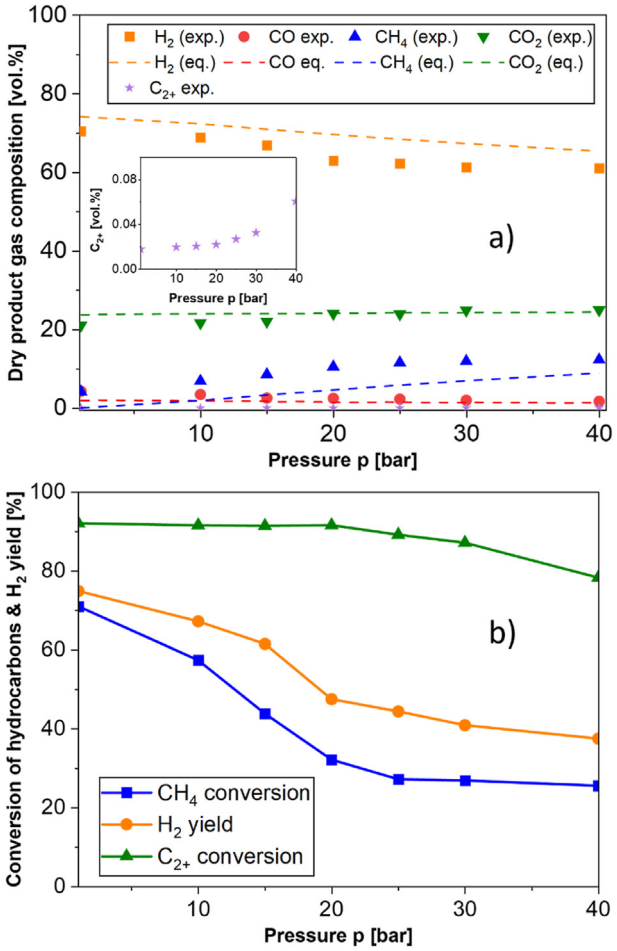

Fig. 7 – a) Product gas composition with pressure in the steam reforming reactor, b) conversion of hydrocarbons and H_2 yield with pressure. The GHSV was 22234 h^{-1}, the feed was the gas produced from SCWG of 8 wt% ethanol (see Table 1), and T 600 °C.

As expected, CH_4 conversion was decreased with pressure, showing a sharper drop at lower pressures than at higher ones, i.e., in the range 25–40 bar, the CH_4 conversion dropped from 27.2% to 25.6%, respectively. A similar trend is observed for the H_2 yield (Eqn 2.2.6). This behavior might be ascribed to the kinetics of the SMR reaction under the high pressure conditions [52,54]. There was a discrepancy between H_2 yield and CH_4 conversion, with the first being higher than the second, at every pressure. This discrepancy was constantly minimized with lower pressure. This behaviour indicates the inhibiting effect of pressure to the SMR and not to WGS which is unaffected. Concerning the concentration of C_{2+} hydrocarbons, there was no notable alteration in their level, with an average value of 0.02 vol%, up to a pressure of 20 bar, and their corresponding conversion rate remained steady at about 92%. Nonetheless, at higher pressures, their conversion rate declined and reached a minimum of roughly 78% with a corresponding concentration of 0.06 vol%. This behaviour could have derived from the favored reverse reaction of ethane hydrogenolysis [55]:

$$C_2H_6 + H_2 \leftrightarrow 2\,CH_4, \Delta H^{298K} \qquad 187\,\frac{kJ}{mol} \qquad (3.6.1)$$

The significance of pressure for the SMR process has already been studied in the literature. Many have used moderate temperature (600 °C) and a pressure up to 15 bar [46,50,56,57]. Others have applied higher temperatures (900 °C) and a maximum pressure of 20 bar [52].

Mosayebi and Nasabi [50] observed a decrease in CH_4 conversion from 57% at 1 bar to 45% at 15 bar using a $LaNiO_3$ perovskite type oxide catalyst for SMR at 600 °C, S/C 1, and GHSV of 900 h^{-1}. In this study, the CH_4 conversion dropped from 70.3% at 1 bar to 45.5% at 15 bar. The higher steam concentration, in this case, likely contributed to the increased CH_4 conversion compared to Mosayebi and Nasabi's equimolar reaction.

Katheria et al. [57] utilized a Ni(15 wt%)/$MgAl_2O_4$ catalyst for SMR at 600 °C with an S/C ratio of 5, reporting CH_4 conversion of approximately 50% at 1 bar, decreasing to about 40% at 10 bar. Jaiswar et al. [56] studied SMR at 600 °C, S/C 5, atmospheric pressure, and 10 bar, using a Ni(15 wt%)/$MgAl_2O_4$ catalyst promoted with Pt. They achieved the highest CH_4 conversion of around 65% at 1 bar with 1 wt% Pt doping, which decreased to approximately 50% at 10 bar. Both studies used a catalyst mass/inlet molar flow of methane ratio of 0.34 $g_{cat}h/mol$, while ours was 14.38 $g_{cat}h/mol$. The results of this work align more closely with Jaiswar et al. [56], likely due to the excess steam and Pt promotion.

Zhang et al. [52] investigated pressure effects (5–20 bar) in a microchannel reactor at 900 °C. At high GHSV (160000–240000 h^{-1}), increasing pressure led to higher CH_4 conversion due to increased contact time between reactants and catalyst. For low GHSVs (40000–80000 h^{-1}) and low pressures (5–10 bar), the higher contact time approached thermodynamic equilibrium, causing a decrease in CH_4 conversion with pressure, following Le Chatelier's principle. However, at the highest GHSV, increasing pressure from 15 to 20 bar did not provide a sufficient contact time increase to reach equilibrium, resulting in decreased CH_4 conversion.

Direct comparison between our study and the literature references is challenging due to different catalyst properties, loading of active metal, and experimental conditions. Nevertheless, all aforementioned studies, and this one, indicate a significant effect of pressure on CH_4 conversion.

3.7. *Characterization of used catalysts*

The TGA MS measurements of the fresh and used catalyst were conducted to examine if any carbon was formed on the catalyst surface. The weight loss of the samples was measured as a function of temperature and is presented in Fig. 8 a). Figure 8 b) shows the gas species detected during the thermal decomposition of the samples. In the temperature range of 100–300 °C, both samples exhibited a decrease in weight, which can be attributed to the release of water vapor [58]. The used catalyst demonstrated more significant weight loss than the fresh catalyst, with three distinct peaks corresponding to water. The first two peaks were observed between temperatures of 100–200 °C and 200–230 °C, respectively, and were related to physisorbed water. The

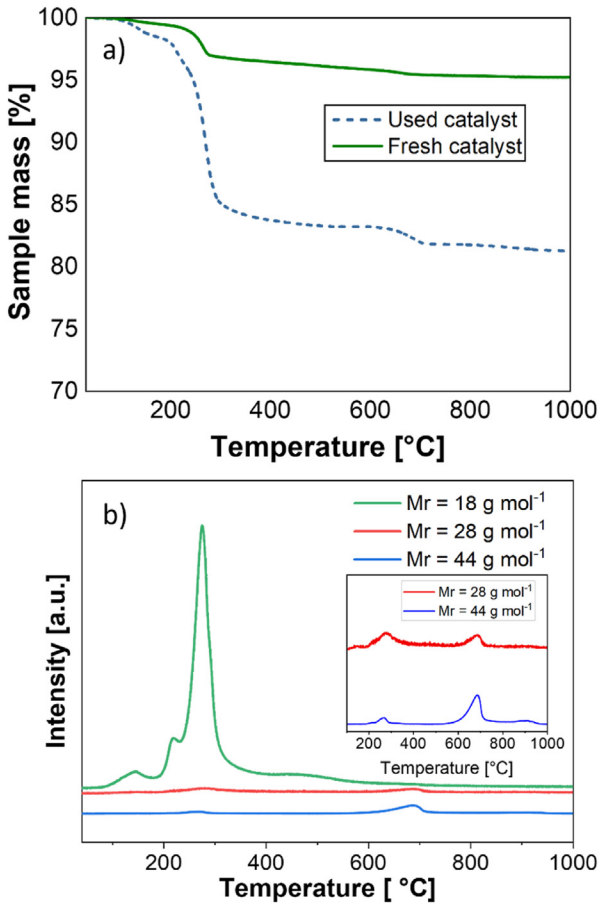

Fig. 8 – a) TGA of the fresh and used catalyst samples and b) respective MS signals of water vapor and carbon oxides. The used catalyst sample had undergone steam reforming of the product gas from SCWG of 8 wt% ethanol. The conditions of steam reforming were 600 °C and 1 atm, with a GHSV of 44557 h^{-1}.

third peak and the most intense peak, observed in the temperature range of 260–280 °C, corresponded to water that was either chemisorbed [59,60] or located in inner catalyst layers [61]. No weight gain was observed in the used catalyst due to re oxidation of Ni atoms, which might be due to partial reoxidation of the catalyst or limited reduction of Ni during reaction [62]. In the temperature range 260–300 °C, two small peaks for CO_2 ad CO were found. As Angeli et al. [8] reported those peaks can be attributed to reactive carbon species. At temperatures between 640 and 700 °C, a slight mass loss of around 1.4% was observed in the used catalyst and was identified as CO_2 and CO. Generally, in this temperature range, the carbon oxides can be formed from the oxidation of filamentous carbon [63]. By analyzing the carbon deposits on the surface of the catalyst, it was calculated that 43.7 mg of carbon had been deposited as coke. This accounts for roughly 0.85% of the total carbon in the feed and corresponds to 17.27 mg of carbon per gram of catalyst (or 17.27 mg_C/g_{cat}).

The low carbon formation could be attributed, on the one hand, to the composition of the catalyst, which incorporated potassium (K). The addition of K has been proven not only to accelerate the rate of the gasification of carbonaceous species but also to prevent their formation [9,64,65]. However, the ample supply of steam during the reaction should be the main factor in avoiding carbon formation. At given temperature and pressure, in an SMR system, the decrease in S/C ratio drives the thermodynamic equilibrium towards carbon formation [28]. Generally, when the steam is in excess it can oxidize the deposited carbon, especially the polymeric species, while it can also inhibit the formation of filamentous carbon [66]. When the carbon content increases so should the S/C ratio otherwise the carbon deposition on the catalyst might increase [6,8]. Choi et al. [67] demonstrated that at medium reforming temperatures (450–500 °C), an S/C ratio >3 can convert almost completely the C_{2+} hydrocarbons in an associated gas with a CH_4/C_{2+} ratio of approx. 4.2, on a Ni–Ru/CGO catalyst. Their long term experiments showed that their catalyst could operate for 900 h under 450 °C and 8.5 bar. Sperle et al. [6] determined the critical S/C ratio for net carbon formation for different mixtures of hydrocarbons with methane, at 500 °C. This value was increasing as the carbon atoms increased from 0.75 with only CH_4 to around 2.8 for $CH_4/C_3H_8/C_3H_6$. They also studied the effect of H_2 addition to a $CH_4/C_3H_8/C_3H_6$ feed. Increasing the H_2/C ratio from 2.7 to 13.4, lower critical S/C ratios were needed. At a H_2/C of 2.7, the critical S/C ratio at 510 °C and 20 bar was 3.5. In the SCWG SMR system of this study, the S/C ratio of the feed to the SMR reactor is above 10 and the respective H_2/C is around 2.38, thus minimizing carbon formation. Nevertheless, the extensive increase in steam may lead to partial deactivation due to sintering of the active metal [68]. Therefore, it was crucial to investigate whether the high amount of steam used in the current process led to the aforementioned phenomena.

Fig. 9 illustrates the XRD patterns of the reduced and used catalyst after steam reforming (at 600 °C, 1 atm, and 5 h on stream) of the product gas from SCWG of 8 wt% ethanol. The patterns of both the reduced and the used catalyst exhibited the same two peaks at 44.5° and 51.8°, which corresponded to

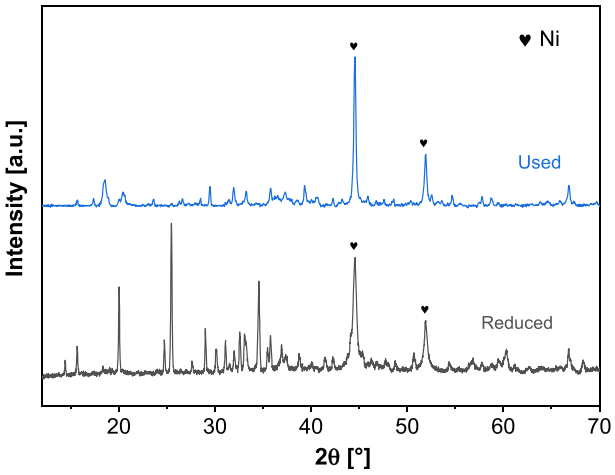

Fig. 9 – XRD graphs of reduced and used catalyst. The used one corresponds to an experiment of steam reforming of the product gas from SCWG of 8 wt% ethanol, at 600 °C, 1 atm and GHSV 44557 h^{-1}.

the (111) and (200) planes of metallic Ni, respectively [69,70]. In the used catalyst, the reduced nickel structure was retained without the appearance of nickel oxides. This outcome can be attributed to the presence of H_2 in the feed of the SMR reactor, which reduces any NiO species formed during the reaction [71,72]. The peaks corresponding to the structure of the support that were identified for the fresh and reduced catalysts in Fig. 3 were not present in the XRD pattern of the used catalyst. Nevertheless, under 5 h of TOS, the catalyst did not show any signs of deactivation.

Furthermore, the XRD peaks of the used catalyst were sharper, suggesting some degree of Ni sintering. Notably, the average size of the Ni crystallites in the used catalyst was estimated to be 53 nm using the Scherrer equation, whereas the size of the reduced catalyst was 35.8 nm. Several factors may lead to sintering, but here an attempt is made to determine only the factors that might have played a role in this case. Temperature is a critical factor in sintering, and increasing the temperature typically results in a higher sintering rate [73–75]. As Christensen et al. [76] reported, the interaction between the active metal and the support also strongly affects the sintering rate of Ni particles via the particle migration mechanism (coalescence). The TPR profile of the catalyst in this study suggests that the metal support interaction is weak, which may have contributed to the sintering of the metal particles. Another factor that can enhance sintering is steam [68,73,76,77]. In this case, the large amount of steam fed to the SMR reactor may have accelerated the sintering rate of the metal particles. However, during the experiments, no deactivation was observed. According to Sehested [73], Ni sintering is a rapid process and quickly reaches a stable state, thereby suggesting that the sintering had taken place before the first measurement of the product gas sample and the recording of the results.

To gain a better understanding of how the reaction affects the oxidation state of Ni, ex situ X ray absorption spectroscopy (XAS) at the Ni K edge was used to measure the fresh and used catalysts (shown in Fig. 10). The normalized X ray absorption near edge structure (XANES) spectra, depicted in Fig. 10 a), give the fingerprint of the oxidation state [78,79]. By comparison of the sample spectrum with Ni foil, NiO and $NiAl_2O_4$ references, the fresh catalyst showed similarities with the NiO reference. This proves the presence of NiO in the initial catalyst, which agrees with the XRD data. The extended X ray absorption fine structure (EXAFS) spectrum (Fig. 10 b) showed Ni–O and Ni–Ni interaction in a radial distance corresponding to NiO. The spent catalyst after steam reforming had similarities with metallic Ni. However, a slight increase in the normalized absorbance in the range 8340–8360 eV was visible, which might be ascribed to surface NiO. The linear combination fitting (LCF) gave a fraction of 86% metallic Ni and a fraction of 14% NiO. In the EXAFS spectrum, a peak at a radial distance of 2.2 Å was observed, which is assigned to first shell Ni–Ni contribution, giving evidence for the predominantly metallic state of the catalyst after the reaction.

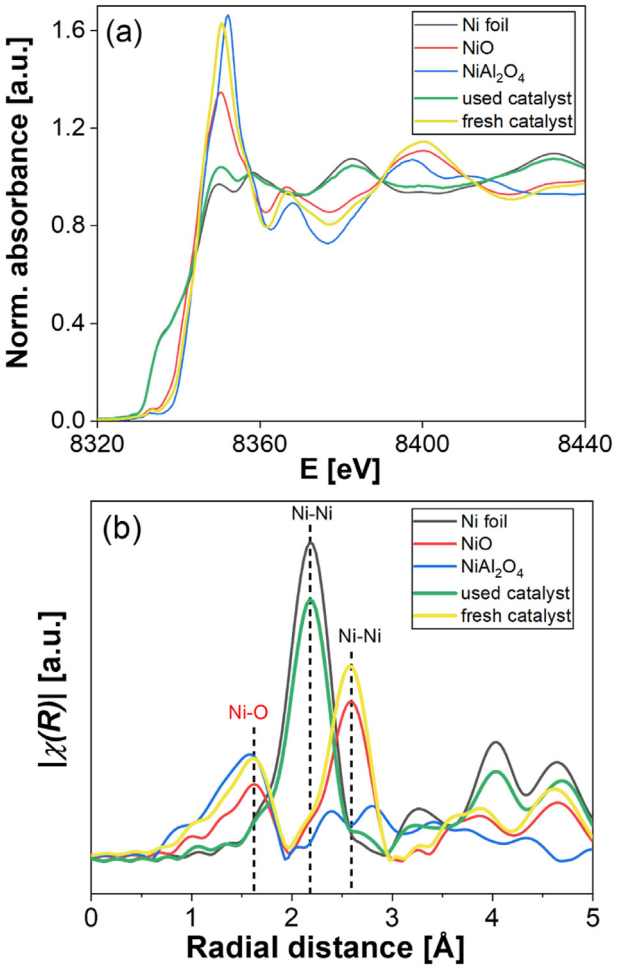

Fig. 10 – a) Normalized ex-situ XANES spectra of fresh and used catalyst at room conditions, b) Fourier transformed EXAFS spectra of the used and fresh catalyst at room conditions. The spectra are compared with the ones of metallic Ni, NiO and $NiAl_2O_4$.

3.8. *Long-time experiment*

Characterization of the used catalyst revealed that the catalyst remained reduced during the reaction, did not suffer from severe carbon deposition but sintering of the active metal was not avoided. These did not have any noticeable effect on the catalyst activity during the short TOS of 5 h, however, a long time experiment would provide solid evidence of any possible deactivation. Therefore, an experiment of 75 h was conducted at 600 °C and ambient pressure (Fig. 11). During the first 48 h the composition of the product gas and the CH_4 conversion were stable, accounting for 84.05% of converted CH_4, 71.8 vol% H_2, 2.1 vol% CO, 2.4 vol% CH_4 and 23.7 vol% CO_2. However, a slight activity loss can be observed after 49 h of operation, which is depicted through a gradual decrease in CH_4 conversion from 49 h to 54 h. Afterwards the CH_4 conversion reached an average value of 77.5% for the rest TOS. Respectively, the concentration of CH_4 increased to 3.4 vol%, CO decreased to 1.9 vol% and H_2 decreased to 70.6 vol%. Similarly, the concentration of heavier hydrocarbons was found to be 0.001 vol% during the first 49 h, whereas afterwards their concentration increased to 0.009 vol%.

Based on the observed changes in these values, it appears that the catalyst's activity in the steam methane reforming

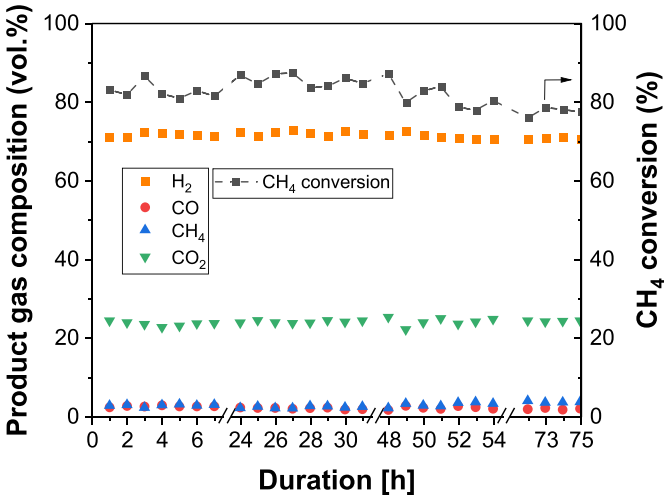

Fig. 11 – Steam reforming of the gas produced from SCWG of 8 wt% ethanol. The conditions of the SCWG were 250 bar and 600 °C, the residence time was 1.5 min. The conditions of steam reforming were 600 °C, ambient pressure and GHSV of approx. 25000 h $^{-1}$.

reaction has slightly deteriorated. Fig. 12 a) depicts the TGA measurement of the catalyst, with only a small increase in weight of 1.55% at 470 °C, possibly due to reoxidation of Ni. This weight increase is related to around 40% of the reduced Ni before the feed introduction, becoming reoxidized after the reaction. Afterwards, the catalyst loses around 1.55% of its weight again, returning to its initial weight for the rest of the analysis. This rate of weight loss is similar to the rate found in the catalyst subjected to an experiment of 5 h (1.4% after 5 h of TOS, Fig. 8). However, the amount of fresh catalyst and the total amount of carbon in the feed were different from the 5 h experiment. By MS measurements, this weight loss can be attributed mainly to release of CO_2 with a peak at 500 °C and 600 °C. It was found that this amount of carbon accounted for 0.019% of the total carbon inserted into the second reactor throughout the whole long term experiment. The latter per centage of deposited carbon is very small compared to the one found in the short term experiment (0.85% of total carbon). Besides, the temperature range of carbon occurrence in the latter case is lower than that in the short term experiment. These differences are probably due to the different space ve locity used in these two experiments, in particular the long duration experiment consisted of a lower space velocity, which may have led to the inhibition of carbon formation [80,81] and/or the variations in the rate of carbon deposition as a function of TOS with the higher rates attained during the first hours of operation.

The XRD profile of the used catalyst (Fig. 13) indicates the reduced state of Ni after the reaction but also with sharper peaks, compared to the reduced catalyst from Fig.9, which accounted for an increase in Ni particle size to 75.5 nm. This increase means that during the reaction, the Ni sintering progressed, leading to a reduction in the surface area of the active metal. Since the formation of carbonaceous species on the catalyst was so small, it is proposed that most likely the increased Ni sintering was responsible for the moderate loss of catalyst activity.

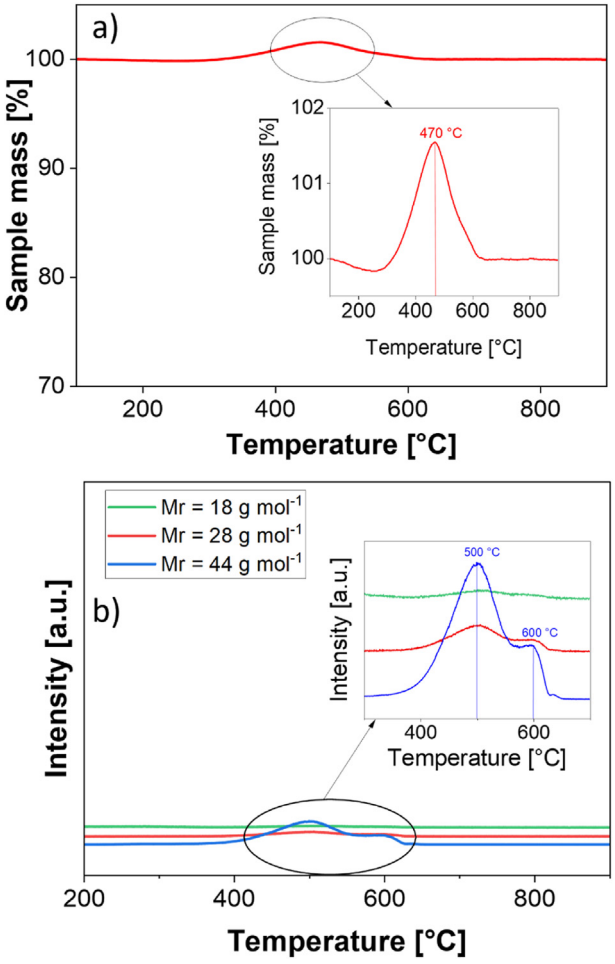

Fig. 12 – a) TGA of the catalyst used in the long-term experiment and b) respective MS signals of water vapor and carbon oxides.

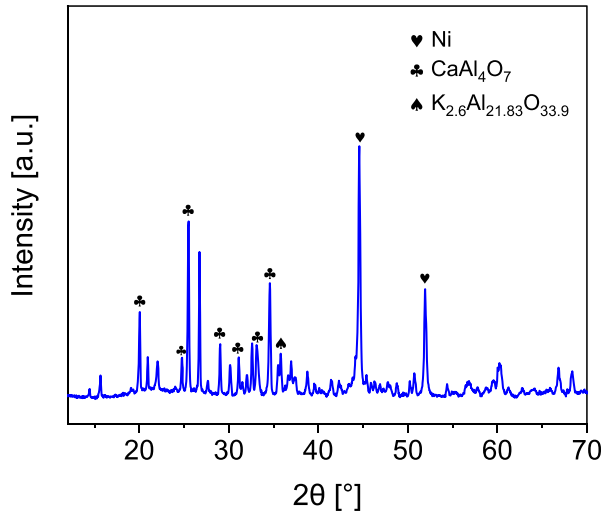

Fig. 13 – XRD profile of the catalyst used in the long-term experiment.

4. Conclusions

This study proposes a novel continuous process for hydrogen production from the product of a supercritical water gasification reactor. The process involves the use of a fixed catalytic bed reactor downstream of the SCWG reactor to carry out steam reforming of the product gas. Ethanol was used in the SCWG reactor, and gasification occurred at 600 °C and 250 bar. A commercial Ni based catalyst was employed in the SMR reactor. The primary objective of this study was the parametric study of the steam reforming reactor to enhance the conversion of methane and carbon monoxide into hydrogen and carbon dioxide while minimizing heavier hydrocarbons traces.

It was found that an increase in temperature brought the product gas closer to thermodynamic equilibrium, with the H_2 concentration reaching approximately 70 vol% and the CH_4 conversion reaching 63.3% at the highest applied temperature of 700 °C. The gas hourly space velocity played a crucial role in the process, with the H_2 concentration in the dry product gas reaching 73.4 vol% and the CH_4 conversion 90.4% at the lowest GHSV of 14852 h^{-1}. At these conditions, the total hydrogen yield based on the ethanol admitted into the system ($Y_{H2,total}$) was approximately 98% with only 27.4% produced in the SCWG reactor and the rest in the steam reformer. The effect of pressure was more profound on CH_4 conversion and H_2 yield at low pressures (1.013 bar–20 bar) than at high pressures, particularly at pressures ranging from 25 bar to 40 bar, due to the kinetics affecting the SMR reaction, under the studied conditions. The excessive steam from the SCWG reactor helped to restrain the formation of carbon with only a low amount of coke found on the catalyst, but it resulted in the sintering of the active metal. The latter phenomenon was responsible for a slight activity loss during 75 h of TOS.

The operating conditions studied in the present work reveal the potential of applying this steam reforming reactor as a pre reforming step. That would mean applying this reactor under mild conditions, e.g., 550–600 °C and 20–30 bar, in order to convert any unwanted side products from the SCWG, like C_{2+} hydrocarbons and CO, into H_2 and CO_2, prior to using a steam methane reformer that would work under higher temperatures.

Overall, this study demonstrated the feasibility of the proposed continuous process, highlighting the importance of the reforming reactor in increasing the hydrogen yield. It also identified potential areas for further optimization to achieve full hydrogen recovery. Further research could involve using different catalysts and more complex feedstocks to better model real wet biomass resources. The optimization could focus on achieving thermodynamic equilibrium at relatively low operating temperatures while minimizing sintering effects.

Funding

This work was supported by the research project: Helmholtz European Partnership for Technological Advancement (HEPTA) [grant agreement no. PIE 0016].

Declaration of competing interest

The authors declare that they have no known competing financial interests or personal relationships that could have appeared to influence the work reported in this paper.

Acknowledgements

The authors would like to thank Dr. Sofia Angeli for her insightful advice and in depth discussions. The authors would also like to thank Mrs. E. Hauer for her contributions to the experimental work and Mr. K. Weiss for his contributions to the mechanical work. The authors acknowledge DESY (Hamburg, Germany), a member of the Helmholtz Association HGF, for the provision of synchrotron light. The measurements were performed at P65 beamline. Finally the authors would like to thank Dmitry Doronkin and Edmund Welter for conducting the measurements.

REFERENCES

[1] Nnabuife SG, Ugbeh Johnson J, Okeke NE, Ogbonnaya C. Present and projected developments in hydrogen production: a technological review*. Carbon Capture Science & Technology Jun. 2022;3:100042. https://doi.org/10.1016/j.ccst.2022.100042.

[2] Osselin F, Soulaine C, Fauguerolles C, Gaucher EC, Scaillet B, Pichavant M. Orange hydrogen is the new green. Nat Geosci 2022;15(10):765 9. https://doi.org/10.1038/s41561 022 01043 9.

[3] Erans M, Sanz Pérez ES, Hanak DP, Clulow Z, Reiner DM, Mutch GA. Direct air capture: process technology, techno economic and socio political challenges. Energy Environ Sci 2022;15(4):1360 405. https://doi.org/10.1039/D1EE03523A.

[4] Rostrup Nielsen JR, Sehested J. Hydrogen and synthesis gas by steam and CO2 reforming. ChemInform Apr. 2003;34(17). https://doi.org/10.1002/chin.200317288.
[5] Levalley TL, Richard AR, Fan M. The progress in water gas shift and steam reforming hydrogen production technologies a review. Int J Hydrogen Energy 2014;39(30):16983 7000. https://doi.org/10.1016/j.ijhydene.2014.08.041.
[6] Sperle T, Chen D, Lødeng R, Holmen A. Pre reforming of natural gas on a Ni catalyst. Criteria for carbon free operation. Appl Catal Gen 2005;282(1 2):195 204. https://doi.org/10.1016/j.apcata.2004.12.011.
[7] Ramakumar KR, Orman S, Kara IB. Pre reformer catalyst in a hydrogen plant. 2020. p. 1 4.
[8] Angeli SD, Pilitsis FG, Lemonidou AA. Methane steam reforming at low temperature: effect of light alkanes' presence on coke formation. Catal Today 2015;242(Part A):119 28. https://doi.org/10.1016/j.cattod.2014.05.043.
[9] Fowles M, Carlsson M. Steam reforming of hydrocarbons for synthesis gas production. Top Catal Dec. 2021;64(17 20):856 75. https://doi.org/10.1007/S11244 021 01496 Z/FIGURES/19.
[10] Ferreira Pinto L, Silva Parizi MP, Carvalho de Araújo PC, Zanette AF, Cardozo Filho L. Experimental basic factors in the production of H2 via supercritical water gasification. Int J Hydrogen Energy 2019;44(47):25365 83. https://doi.org/10.1016/j.ijhydene.2019.08.023.
[11] Lee CS, Conradie AV, Lester E. Review of supercritical water gasification with lignocellulosic real biomass as the feedstocks: process parameters, biomass composition, catalyst development, reactor design and its challenges. Chem Eng J 2021;415. https://doi.org/10.1016/j.cej.2021.128837.
[12] Shan YQ, Yin LX, Djandja OS, Wang ZC, Duan PG. Supercritical water gasification of waste water produced from hydrothermal liquefaction of microalgae over Ru catalyst for production of H2 rich gas fuel. Fuel November 2020;292:2021. https://doi.org/10.1016/j.fuel.2021.120288.
[13] Matsumura Y, et al. Biomass gasification in near and super critical water: status and prospects. Biomass Bioenergy 2005;29(4):269 92. https://doi.org/10.1016/j.biombioe.2005.04.006.
[14] Boukis N, Stoll IK. Gasification of biomass in supercritical water, challenges for the process design lessons learned from the operation experience of the first dedicated pilot. Plant 2021. https://doi.org/10.3390/pr9030455.
[15] Azadi P, Farnood R. Review of heterogeneous catalysts for sub and supercritical water gasification of biomass and wastes. Int J Hydrogen Energy Aug. 2011;36(16):9529 41. https://doi.org/10.1016/J.IJHYDENE.2011.05.081.
[16] Gao N, Li A, Quan C, Gao F. Hydrogen rich gas production from biomass steam gasification in an updraft fixed bed gasifier combined with a porous ceramic reformer. Int J Hydrogen Energy 2008;33(20):5430 8. https://doi.org/10.1016/j.ijhydene.2008.07.033.
[17] Gao N, Li A, Quan C. A novel reforming method for hydrogen production from biomass steam gasification. Bioresour Technol 2009;100(18):4271 7. https://doi.org/10.1016/j.biortech.2009.03.045.
[18] Zhang J, Wang M, Xu S, Feng Y. Hydrogen and methane mixture from biomass gasification coupled with catalytic tar reforming, methanation and adsorption enhanced reforming. Fuel Process Technol Sep. 2019;192:147 53. https://doi.org/10.1016/J.FUPROC.2019.04.023.
[19] Shien R, Amran T, Abdullah T, Ripin A, Ahmad A, Isa K. Hydrogen rich gas production by steam reforming of gasified biomass tar over Ni/dolomite/La2O3 catalyst. J Environ Chem Eng 2019:103490. https://doi.org/10.1016/j.jece.2019.103490. no. September.
[20] Gao N, Wang X, Li A, Wu C, Yin Z. Hydrogen production from catalytic steam reforming of benzene as tar model compound of biomass gasification. Fuel Process Technol 2016;148:380 7. https://doi.org/10.1016/j.fuproc.2016.03.019.
[21] Xu M, et al. Steam reforming of biomass gasification tar over Ni based catalyst supported by TiO2 SiO2 composite. Fuel Jul. 2023;343:127934. https://doi.org/10.1016/J.FUEL.2023.127934.
[22] Grams J, Ryczkowski R, Sadek R, Chałupka Śpiewak K, Casale S, Dzwigaj S. Enhanced activity of NiZrBEA catalyst for upgrading of biomass pyrolysis vapors to H2 rich gas. Int J Hydrogen Energy Sep. 2022;47(82):34909 23. https://doi.org/10.1016/j.ijhydene.2022.08.082.
[23] Sun Y, et al. Biomass Derived low concentration CO2 mixed Gas Combined Steam to Reform Methane through Ni based volcanic rock catalyst. Int J Hydrogen Energy 2022;47(55):23139 50. https://doi.org/10.1016/j.ijhydene.2022.05.065.
[24] Rahbari A, Shirazi A, Venkataraman MB, Pye J. Solar fuels from supercritical water gasification of algae: impacts of low cost hydrogen on reformer configurations. Appl Energy Apr. 2021;288:116620. https://doi.org/10.1016/j.apenergy.2021.116620.
[25] Ruya PM, Lim SS, Purwadi R, Zunita M. Sustainable hydrogen production from oil palm derived wastes through autothermal operation of supercritical water gasification system. Energy Oct. 2020;208:118280. https://doi.org/10.1016/J.ENERGY.2020.118280.
[26] Zhang C, Li Y, Chu Z, Fang Y. Thermodynamic analysis of integrated sorption enhanced staged gasification of biomass and in situ CO2 utilization by methane reforming process based on calcium looping. Energy Convers Manag Feb. 2023;278:116710. https://doi.org/10.1016/j.enconman.2023.116710.
[27] Hantoko D, et al. Thermodynamic study on the integrated supercritical water gasification with reforming process for hydrogen production: effects of operating parameters. Int J Hydrogen Energy 2018;43(37):17620 32. https://doi.org/10.1016/j.ijhydene.2018.07.198.
[28] Angeli SD, Monteleone G, Giaconia A, Lemonidou AA. State of the art catalysts for CH4 steam reforming at low temperature. Int J Hydrogen Energy 2014;39(5):1979 97. https://doi.org/10.1016/j.ijhydene.2013.12.001.
[29] Angeli SD, Turchetti L, Monteleone G, Lemonidou AA. Catalyst development for steam reforming of methane and model biogas at low temperature. Appl Catal, B 2016;181:34 46. https://doi.org/10.1016/j.apcatb.2015.07.039.
[30] Kechagiopoulos PN, Angeli SD, Lemonidou AA. Low temperature steam reforming of methane: a combined isotopic and microkinetic study. Appl Catal, B May 2017;205:238 53. https://doi.org/10.1016/J.APCATB.2016.12.033.
[31] Schädel BT, Duisberg M, Deutschmann O. Steam reforming of methane, ethane, propane, butane, and natural gas over a rhodium based catalyst. Catal Today Apr. 2009;142(1 2):42 51. https://doi.org/10.1016/J.CATTOD.2009.01.008.
[32] Aasberg Petersen K, Dybkjær I, Ovesen CV, Schjødt NC, Sehested J, Thomsen SG. Natural gas to synthesis gas catalysts and catalytic processes. J Nat Gas Sci Eng 2011;3(2):423 59. https://doi.org/10.1016/j.jngse.2011.03.004.
[33] Chaubey R, Sahu S, James OO, Maity S. A review on development of industrial processes and emerging techniques for production of hydrogen from renewable and sustainable sources. Renew Sustain Energy Rev 2013;23:443 62. https://doi.org/10.1016/j.rser.2013.02.019.
[34] Rostrup Nielsen JR, Sehested J, Nørskov JK. Hydrogen and synthesis gas by steam and C02 reforming. Adv Catal Jan.

2002;47:65 139. https://doi.org/10.1016/S0360 0564(02) 47006 X.
[35] Byrd AJ, Pant KK, Gupta RB. Hydrogen production from ethanol by reforming in supercritical water using Ru/Al2O3 catalyst. Energy Fuel Nov. 2007;21(6):3541 7. https://doi.org/10.1021/EF700269Z.
[36] Sinağ A, Kruse A, Rathert J. Influence of the heating rate and the type of catalyst on the formation of key intermediates and on the generation of gases during hydropyrolysis of glucose in supercritical water in a batch reactor. Ind Eng Chem Res 2004;43(2):502 8. https://doi.org/10.1021/ie030475+.
[37] Habicht W, Boukis N, Hauer E, Dinjus E. Analysis of hydrothermally formed corrosion layers in Ni base alloy 625 by combined FE SEM and EDXS. X RAY Spectrometry; 2011.
[38] Lemonidou AA, Goula MA, Vasalos IA. Carbon dioxide reforming of methane over 5 wt.% nickel calcium aluminate catalysts effect of preparation method. Catal Today Nov. 1998;46(2 3):175 83. https://doi.org/10.1016/S0920 5861(98) 00339 3.
[39] Li C, Chen YW. Temperature programmed reduction studies of nickel oxide/alumina catalysts: effects of the preparation method. Thermochim Acta Jun. 1995;256(2):457 65. https://doi.org/10.1016/0040 6031(94)02177 P.
[40] Chatterjee R, Banerjee S, Banerjee S, Ghosh D. Reduction of nickel oxide powder and pellet by hydrogen. Trans Indian Inst Met Jun. 2012;65(3):265 73. https://doi.org/10.1007/s12666 012 0130 0.
[41] Ranjbar A, Rezaei M. Dry reforming reaction over nickel catalysts supported on nanocrystalline calcium aluminates with different CaO/Al2O3 ratios. J Nat Gas Chem Mar. 2012;21(2):178 83. https://doi.org/10.1016/S1003 9953(11) 60351 4.
[42] Chattanathan SA, Adhikari S, McVey M, Fasina O. Hydrogen production from biogas reforming and the effect of H2S on CH4 conversion. Int J Hydrogen Energy 2014;39(35):19905 11. https://doi.org/10.1016/j.ijhydene.2014.09.162.
[43] Ratnasamy C, Wagner J. Water gas shift catalysis. Catal Rev Sci Eng 2009;51(3):325 440. https://doi.org/10.1080/01614940903048661.
[44] Xu J, Froment GF. Methane steam reforming, methanation and water gas shift: I. Intrinsic kinetics. AIChE J Jan. 1989;35(1):88 96. https://doi.org/10.1002/aic.690350109.
[45] Obradović AO, Likozar B, Levec J. Steam methane reforming over Ni based pellet type and Pt/Ni/Al 2 O 3 structured plateplate type catalyst. Intrinsic Kinetics Study 2013. https://doi.org/10.1021/ie401551m.
[46] Abbas SZ, Dupont V, Mahmud T. Kinetics study and modelling of steam methane reforming process over a NiO/Al2O3 catalyst in an adiabatic packed bed reactor. Int J Hydrogen Energy Feb. 2017;42(5):2889 903. https://doi.org/10.1016/J.IJHYDENE.2016.11.093.
[47] Yang X, Da J, Yu H, Wang H. Characterization and performance evaluation of Ni based catalysts with Ce promoter for methane and hydrocarbons steam reforming process. Fuel 2016;179:353 61. https://doi.org/10.1016/j.fuel.2016.03.104.
[48] Mosayebi A, Nasabi M. Steam methane reforming on LaNiO 3 perovskite type oxide for syngas production, activity tests, and kinetic modeling. 2020. https://doi.org/10.1002/er.5300.
[49] Ahmed S, Lee SHD, Ferrandon MS. Catalytic steam reforming of biogas effects of feed composition and operating conditions. Int J Hydrogen Energy 2015;40(2):1005 15. https://doi.org/10.1016/j.ijhydene.2014.11.009.
[50] Mosayebi A, Nasabi M. Steam methane reforming on LaNiO3 perovskite type oxide for syngas production, activity tests, and kinetic modeling. Int J Energy Res Jun. 2020;44(7):5500 15. https://doi.org/10.1002/ER.5300.
[51] Zhai X, Cheng Y, Zhang Z, Jin Y, Cheng Y. Steam reforming of methane over Ni catalyst in micro channel reactor. Int J Hydrogen Energy Jun. 2011;36(12):7105 13. https://doi.org/10.1016/j.ijhydene.2011.03.065.
[52] Zhang N, Chen X, Chu B, Cao C, Jin Y, Cheng Y. Catalytic performance of Ni catalyst for steam methane reforming in a micro channel reactor at high pressure. Chemical Engineering and Processing Process Intensification 2017;118:19 25. https://doi.org/10.1016/j.cep.2017.04.015.
[53] Farshchi Tabrizi F, Mousavi SAHS, Atashi H. Thermodynamic analysis of steam reforming of methane with statistical approaches. Energy Convers Manag Oct. 2015;103:1065 77. https://doi.org/10.1016/J.ENCONMAN.2015.07.005.
[54] Rostrup Nielsen JR. Activity of nickel catalysts for steam reforming of hydrocarbons. J Catal 1973;31:173 99.
[55] Taylor WF, Sinfelt JH, Yates DJC. Catalysis over supported metals. IV. Ethane hydrogenolysis over dilute nickel catalysts. J Phys Chem 1965;69(11):3857 63. https://doi.org/10.1021/J100895A036/ASSET/J100895A036.FP.PNG V03.
[56] Jaiswar VK, Katheria S, Deo G, Kunzru D. Effect of Pt doping on activity and stability of Ni/MgAl2O4 catalyst for steam reforming of methane at ambient and high pressure condition. Int J Hydrogen Energy 2017;42(30):18968 76. https://doi.org/10.1016/j.ijhydene.2017.06.096.
[57] Katheria S, Gupta A, Deo G, Kunzru D. Effect of calcination temperature on stability and activity of Ni/MgAl2O4 catalyst for steam reforming of methane at high pressure condition. Int J Hydrogen Energy 2016;41(32):14123 32. https://doi.org/10.1016/j.ijhydene.2016.05.109.
[58] Świrk K, Rønning M, Motak M, Beaunier P, Da Costa P, Grzybek T. Ce and Y modified double layered hydroxides as catalysts for dry reforming of methane: on the effect of yttrium promotion. Catalysts 2019;9(1). https://doi.org/10.3390/catal9010056.
[59] Dou B, Dupont V, Pan W, Chen B. Removal of aqueous toxic Hg(II) by synthesized TiO2 nanoparticles and TiO2/montmorillonite. Chem Eng J Jan. 2011;166(2):631 8. https://doi.org/10.1016/J.CEJ.2010.11.035.
[60] Jiang B, et al. Highly dispersed Ni/montmorillonite catalyst for glycerol steam reforming: effect of Ni loading and calcination temperature. Appl Therm Eng Oct. 2016;109:99 108. https://doi.org/10.1016/J.APPLTHERMALENG.2016.08.041.
[61] Parker LM, Milestone NB, Newman RH. The use of hydrotalcite as an anion absorbent. Ind Eng Chem Res 1995;34:1196 202 [Online]. Available: https://pubs.acs.org/sharingguidelines. [Accessed 21 March 2023].
[62] Vogt C, Kranenborg J, Monai M, Weckhuysen BM. Structure sensitivity in steam and dry methane reforming over nickel: activity and carbon formation. ACS Catal 2020;10(2):1428 38. https://doi.org/10.1021/acscatal.9b04193.
[63] Świrk K, et al. Carbon resistant NiO Y2O3 nanostructured catalysts derived from double layered hydroxides for dry reforming of methane. Catal Today 2021;366. https://doi.org/10.1016/j.cattod.2020.03.032.
[64] Lin B, et al. Deactivation study of carbon supported ruthenium catalyst with potassium promoter. Appl Catal Gen Jul. 2017;541:1 7. https://doi.org/10.1016/J.APCATA.2017.04.020.
[65] Carlsson M. Carbon formation in steam reforming and effect of potassium promotion. Johnson Matthey Technology Review 2015;59(4):313 8. https://doi.org/10.1595/205651315X688992.
[66] Zhao Q, et al. Steam reforming of CH4 at low temperature on Ni/ZrO2 catalyst: effect of H2O/CH4 ratio on carbon deposition. Int J Hydrogen Energy May 2020;45(28):14281 92. https://doi.org/10.1016/j.ijhydene.2020.03.112.

[67] Choi S, Bae J, Lee S, Oh J, Katikaneni SP. Pre reforming of higher hydrocarbons contained associated gas using a pressurized reactor with a Ni19.5 Ru0.05/CGO catalyst. Chem Eng Sci 2017;168:15 22. https://doi.org/10.1016/j.ces.2017.04.033.
[68] Prasad DH, et al. Effect of steam content on nickel nano particle sintering and methane reforming activity of Ni CZO anode cermets for internal reforming SOFCs. Appl Catal Gen Jan. 2012;411 412:160 9. https://doi.org/10.1016/J.APCATA.2011.10.035.
[69] Rouquette J, et al. High pressure structural and vibrational study of PbZr 0.40Ti0.60O3. Inorg Chem Nov. 2008;47(21):9898 904. https://doi.org/10.1021/IC8008688/ASSET/IMAGES/LARGE/IC 2008 008688 0008.JPEG.
[70] Suh IK, Ohta H, Waseda Y. High temperature thermal expansion of six metallic elements measured by dilatation method and X ray diffraction. J Mater Sci Feb. 1988;23(2):757 60. https://doi.org/10.1007/BF01174717/METRICS.
[71] Hashemnejad SM, Parvari M. Deactivation and regeneration of nickel based catalysts for steam methane reforming. Chin J Catal Jan. 2011;32(1 2):273 9. https://doi.org/10.1016/S1872 2067(10)60175 1.
[72] Ioannidou G, Loukia Yfanti V, Lemonidou AA. Optimization of reaction conditions for hydrodeoxygenation of bio glycerol towards green propylene over molybdenum based catalyst. Catal Today 2022. https://doi.org/10.1016/j.cattod.2022.09.008. no. September.
[73] Sehested J. Sintering of nickel steam reforming catalysts. J Catal Jul. 2003;217(2):417 26. https://doi.org/10.1016/S0021 9517(03)00075 7.
[74] Christensen KO, Chen D, Lødeng R, Holmen A. Effect of supports and Ni crystal size on carbon formation and sintering during steam methane reforming. Appl Catal Gen Oct. 2006;314(1):9 22. https://doi.org/10.1016/J.APCATA.2006.07.028.
[75] S. Tsyganov, J. Kästner, B. Rellinghaus, T. Kauffeldt, F. Westerhoff, and D. Wolf, "Analysis of Ni nanoparticle gas phase sintering", doi: 10.1103/PhysRevB.75.045421.
[76] Christensen KO, Chen D, Lødeng R, Holmen A. Effect of supports and Ni crystal size on carbon formation and sintering during steam methane reforming. Appl Catal Gen Oct. 2006;314(1):9 22. https://doi.org/10.1016/J.APCATA.2006.07.028.
[77] Iglesias I, Baronetti G, Mariño F. Ni/Ce0.95M0.05O2 d (M = Zr, Pr, La) for methane steam reforming at mild conditions. Int J Hydrogen Energy 2017;42(50):29735 44. https://doi.org/10.1016/j.ijhydene.2017.09.176.
[78] Mutz B, Carvalho HWP, Mangold S, Kleist W, Grunwaldt JD. Methanation of CO2: structural response of a Ni based catalyst under fluctuating reaction conditions unraveled by operando spectroscopy. J Catal Jul. 2015;327:48 53. https://doi.org/10.1016/J.JCAT.2015.04.006.
[79] Schmitt CC, Zimina A, Fam Y, Raffelt K, Grunwaldt JD, Dahmen N. Evaluation of high loaded Ni based catalysts for upgrading fast pyrolysis bio oil. Catalysts Sep. 2019;9(9):784. https://doi.org/10.3390/CATAL9090784. 2019, Vol. 9, *Page* 784.
[80] Robertson SD. carbon formation from methane pyrolysis over some transition metal surfaces I. Nature and properties of the carbons formed. Carbon N Y 1970;8:365 74.
[81] Rostrupnielsen J. Mechanisms of carbon formation on nickel containing catalysts. J Catal Jun. 1977;48(1 3):155 65. https://doi.org/10.1016/0021 9517(77)90087 2.